Simulated Yeast with Mobile Polarity Sites Is More Sensitive to Pheromone Gradients

By

Kaiyun Guan

Senior Honors Thesis
Department of Chemistry
University of North Carolina at Chapel Hill

04/10/2019

Approved:

_____

Dr. Timothy Elston, Thesis Advisor

Dr. Bo Li, Reader

Dr. Brian Hogan. Reader

ABSTRACT

Cell polarity is the asymmetric distribution of cellular components and molecules. It is crucially important for effective cell motility and other directional functions. However, practically all types of cells were exposed in a large amount of molecular noise which interfered cell polarity, leading the cells to polarize in the wrong direction. Interestingly, though exposed in molecular noise, yeast cells can usually find and polarize in the direction of extracellular pheromone gradients during mating. This study investigated how yeast cells decoded the extracellular pheromone gradient to polarize in the right direction despite the noise. With particle-based simulations, we found that exposed to a shallow signal gradient, the simulated yeast with mobile polarity sites interpreted the direction of the signal more accurately than the one with static polarity sites. Therefore, the highly dynamic polarity sites could help yeast cells to decode the extracellular pheromone gradient against molecular noise. Future study will focus on adding more complex signaling pathways to the simulated yeast models to further investigate the effect of mobile polarity sites on yeast polarity establishment.

INTRODUCTION

Cell polarity is the asymmetric distribution of cellular components and molecules. It is essential for effective cell motility and other directional functions like neuronal signaling, transport across epithelia, and specification of body axes in developing embryos[1,2,3]. Interpreting a gradient of an external chemoattractant is a common and important way to orient polarity in the correct direction[4]. Cells contain receptors that transmit a signal to the cell interior upon binding chemoattractant. Each cell uses this information to determine which region of its surface is exposed to maximal chemoattractant. Finally, the cell transmits this information to the final effectors responsible for polarization[5]. In many contexts, such as migrating neutrophils, mating yeast, and aggregating slime molds, this sophisticated process involves G protein-coupled receptors (GPCRs) intrinsically linked to the activation of Rho GTPases and their cytoskeleton remodeling effectors[6,7,8].

In the process of polarization directed by external chemoattractant, a cell needs to establish a polarity site that corresponds to the direction of the chemoattractant gradient. A polarity site is a defined region of the plasma membrane where signaling molecules are concentrated to regulate polarization. Positive feedback is a common way to enhance polarity site establishment[9]. Specifically, polarized distribution of upstream signaling molecules leads to polarized distribution of downstream molecules, and polarized downstream molecules confine the upstream signaling molecules in a certain region of the plasma membrane through positive feedback. In this way, positive feedback enables the cell to accelerate localized recruitment in the direction of the extracellular chemoattractant[9].

The yeast *Saccharomyces cerevisiae* is an ideal model for studying eukaryotic cell polarity. Due to their microscopic size and simple growth requirements, yeast cells are inexpensive and easy to grow in the laboratory[10]. Yeast genes have been well characterized, and yeast gene expression can be easily manipulated. Many of the genes that control the establishment of cell polarity are proved to be conserved between yeast and more complex eukaryotic organisms[11]. For example, Cdc42 is a pivotal component of the polarity machinery in yeast, and it is conserved throughout the evolution of the metazoa[12]. While mating, a yeast cell will sense and polarize toward the pheromone gradient released by another yeast cell. When pheromone α factors bind to pheromone α factor receptors (Ste2), which are G-protein coupled receptors (GPCRs), Ste2 activates Gα to dissociate from Gβγ. Gβγ binds to an adaptor protein Far1 linked with Cdc24, which is Cdc42's guanine nucleotide exchange factor (GEF). Then, the Far1-Cdc24-G protein complex will activate Cdc42-GDP by catalyzing the exchange of GDP for GTP. This is the main pathway by which yeast cells decode the pheromone gradient. Yeast cells have another pathway to strengthen local activation of Cdc42, thus enabling the polarization of active Cdc42. Specifically, Cdc42-GTP recruits the scaffold protein Bem1 associated with Cdc24. The recruitment of Bem1-Cdc24 results in localized activation of Cdc42. Cdc42-GTP will then recruit more Bem1-Cdc24 and activate more Cdc42-GDP via positive feedback. This pathway ensures the formation of a stable polarized patch to initiate yeast cell polarization. Finally, activated Cdc42 will stimulate polarized organization of the actin cytoskeleton and membrane trafficking systems. Cdc42 forms a "polar cap" and actin cables become oriented for targeted

secretion. Concentrated actin network at the polar cortex leads to formation of a mating projection[11].

However, yeast cells sense and respond to external cues in a noisy environment. Specifically, molecular noise includes the random movement of molecules, the probabilistic behavior of chemical reactions, and the competition between different signaling pathways. Cells must filter the signal from noise, process the relevant information, and then mount the appropriate response.[13] Interestingly, since a yeast cell has a very small size compared with other cell types, only about 4 - 5 μm in diameter[10], it can be harder for a yeast cell to sense the difference in the concentration of extracellular chemoattractant gradients. Previous studies have shown that yeast cells could sense the direction of a pheromone gradient with a 2.5 nM concentration difference across the cell, despite only a difference of 0.5% in the concentration of pheromone molecules bound to the receptors from the cell front and back[14,15]. Moreover, differences in the receptor (Ste2) occupancy estimated to be about 1% were sufficient for orientation toward the pheromone gradient.[16] Additionally, modeling of receptor-pheromone binding interactions suggests that the resulting gradient is noisy, with a difference of 45±50 pheromone-bound receptors between the front and the back[17]. It remains a secret how yeast cells decode shallow extracellular pheromone gradients despite molecular noise. To investigate this question, we established 3D computational models of yeast cells that reveal spatio-temporal information of signaling molecules involved in yeast polarity. We adopted the particle-based simulations to investigate the role of stochastic effects in models of yeast polarity establishment. Particle-based approaches describe molecular noise better than macroscopic, coarser-grained approaches such as Gillespie or stochastic PDE-based approaches.[18] Furthermore, particle-based approaches can more accurately simulate diffusion-limited second-order reactions that occur on membranes, which are abundant in models of yeast polarity establishment. With particle-based simulations, we found that exposed to a shallow signal gradient, the simulated yeast with a mobile polarity site interpreted the direction of the signal more accurately than the one with a static polarity site.

RESULTS

Our model consisted of two pathways that activated cytosolic or membrane Cdc42 (Fig. 1). One pathway involved Bem1-Cdc24 complex, while the other involved Far1-Cdc24 complex. In our study, Far1-Cdc24 associated with G$\beta\gamma$ was denoted as FarGEFGa and Bem1-Cdc24 as BemGEF. Instead of establishing an extracellular pheromone gradient, our simplified model constructed a gradient of membrane FarGEFGa for practical reasons. The gradient direction was from the back of the cell with negative X coordinates to the front of the cell with positive X coordinates. We tested yeast polarity activity respectively under a uniform (back : front ≈ 5:5), shallow (back : front ≈ 4:6), or strong (back : front ≈ 1:9) gradient. We performed 90 simulations for each gradient set. We set the simulation time to 500 seconds, which should be sufficient for full polarization[19].

In the present study, we defined a cluster of activated Cdc42 molecules as a polarity site. Interestingly, studies have shown that the polarity sites in yeast cells kept wandering for several minutes before fully polarized[20,21,22,23]. To investigate the effect of this "wandering" behavior on yeast cell polarity, we established two kinds of models. In one model, both cytosolic and membrane Cdc42 could be activated. This model was denoted as "mobile model" since the polarity sites were highly dynamic and wandered prior to full polarization (Fig. 4A). The other model where only membrane Cdc42 could be activated was denoted as the "static model" because the polarity sites almost did not move or wander once formed (Fig. 4B). The parameters of the models are listed in Table 1 & 2 in *Models & Methods*.

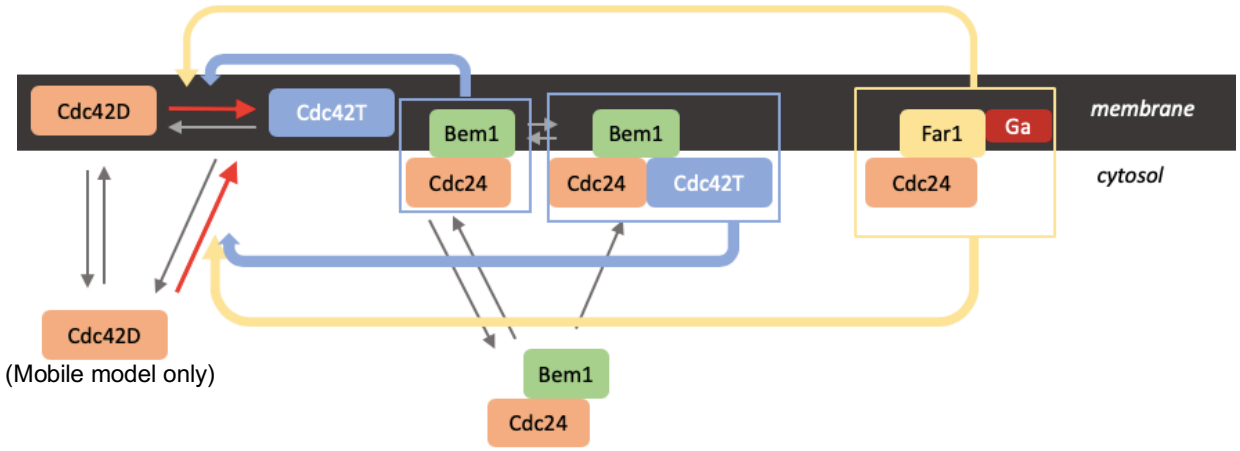

Figure 1. Signaling networks in our models. Ga: free Gβγ. Cdc42D: Cdc24-GDP. Cdc42T: Cdc42-GTP. Yellow arrow: activation of Cdc42 by Far1-Cdc24-Gβγ. Blue arrow: activation of Cdc42 by Bem1-Cdc24 or Bem1-Cdc24 associated with activated Cdc42.

We distinguished between polarized realizations and incompletely polarized realizations with the Ripley's K function[24]. The Ripley's K function has been used frequently to study clustering in biology.[25,26] It is a spatial analysis method used to describe how point patterns occur over a given area of interest. A larger value of *K(d)* indicated a more concentrated polarity site. In our study, the function was used to determine whether the activated Cdc42 were concentrated at a certain part of the cell. After visual inspection, we defined mobile simulations with $K(1.25) \geq 20$ and static simulations with $K(2.25) \geq 20$ as mature polarization. Interestingly, the polarity sites in simulated cells of mobile models were smaller than those in static models (Fig. 2, red spheres). Polarized cells in mobile models had patches with an average base radius of 1.20 μm, which was much smaller than the base radius (1.96 μm) in the static models. .

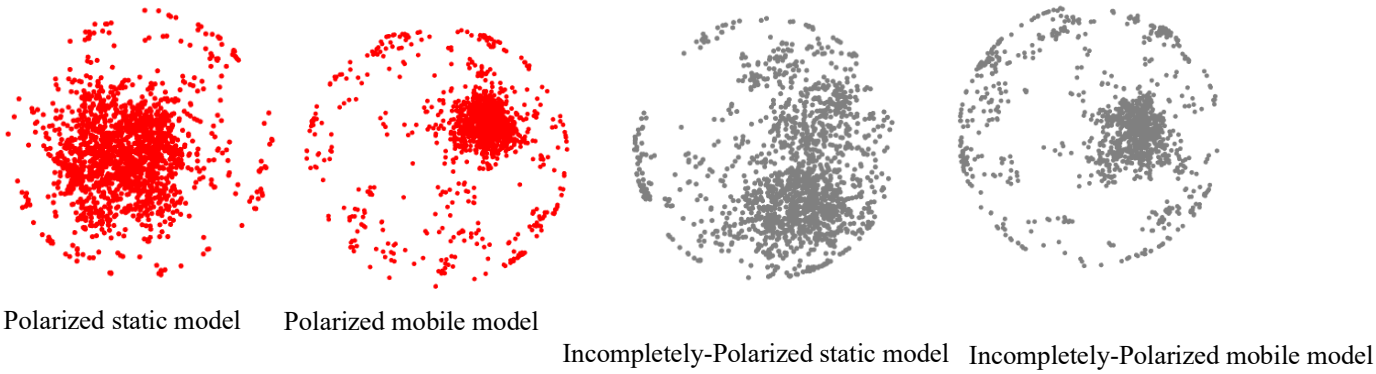

Figure 2. Polarity sites in the static or mobile models with FarGEFGa gradients. Red spheres: activated Cdc42 distribution in the polarized yeast. Gray spheres: activated Cdc42 distribution in the yeast incompletely polarized according to our K-function threshold.

To analyze whether the polarity sites were aligned with FarGEFGa gradients, we measured the angles between the gradient direction and the polarity direction (polarity angles) (Fig. 3). A zero-degree polarity angle meant that the polarity direction completely aligned with the gradient, whereas a 180-degree polarity angle indicated the polarity direction opposite of the gradient. Simulated cells in both the static and mobile models polarized to a random direction under a

uniform gradient. Also, simulated cells in both models successfully polarized in the direction of a 1:9 gradient. A highly significant difference occurred between the two models under a 4:6 gradient. In static models under a 4:6 gradient, the average angle was 92.75 °, indicating failure to respond to the gradient. By contrast, in mobile models, 46.2% (24 in 52) of the polarity angles were below 45°, indicating successful polarization in the appropriate direction. Hence, under a shallow gradient, mobile models decoded the gradient better than the static ones.

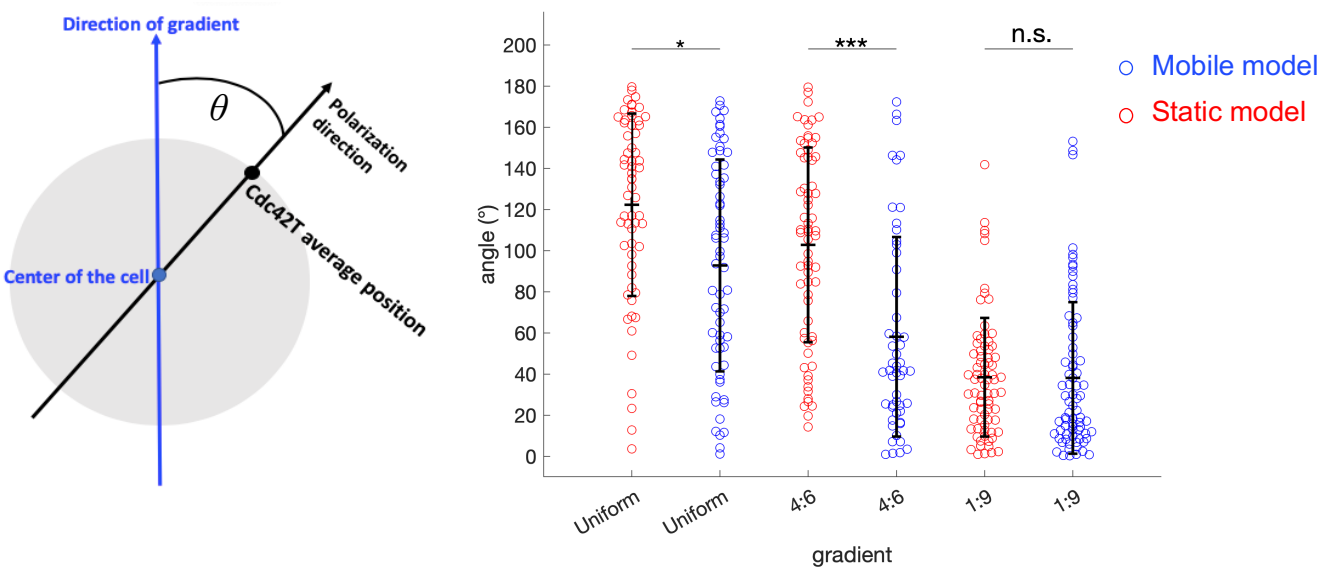

Gradient, model type	Uniform, static	Uniform, mobile	4:6, static	4:6, mobile	1:9, static	1:9, mobile
Number of realizations	61	63	67	52	76	75
Average polarity angle (°)	122.2816	92.7494	102.68	58.09	38.43	38.05

Figure 3. Scatter plots of the angles between the polarity direction and the gradient direction (polarity angles). Each point on the plot represents the polarity angle of a realization. KS test, *: $0.01 < p < 0.05$; **: $0.001 < p < 0.01$; ***: $p < 0.001$. *n.s.*: not significant.

3-D videos were generated to visualize polarity sites at different time points. Here we take the video of a simulation of the mobile model under a 4:6 FarGEFGa gradient as an example (Fig. 4A). Interestingly, the polarity sites wandered for a long time before mature polarization. At 60 s, one site started to dominate but not corresponding to the FarGEFGa gradient. At 100 s, this dominant site disappeared. After 240 s, another site formed closer to the FarGEFGa gradient and disappeared again after a short time. After 450 s, another site whose K value reached 20 grew in

the gradient direction. We defined the 450-second period when polarity sites changed locations before stabilized as the "wandering time". This pattern of wandering polarity was observed in the real biological process of yeast polarization[22,23]. It also occurred in computational models of positive feedback by local activation[20,21]. Nevertheless, in static models, the polarity sites almost did not move once formed (Fig. 4B). Coupled with the polarity angle analysis in Fig 3., wandering polarity sites might actually help the yeast to decode pheromone gradient and polarize in the right direction.

(A)

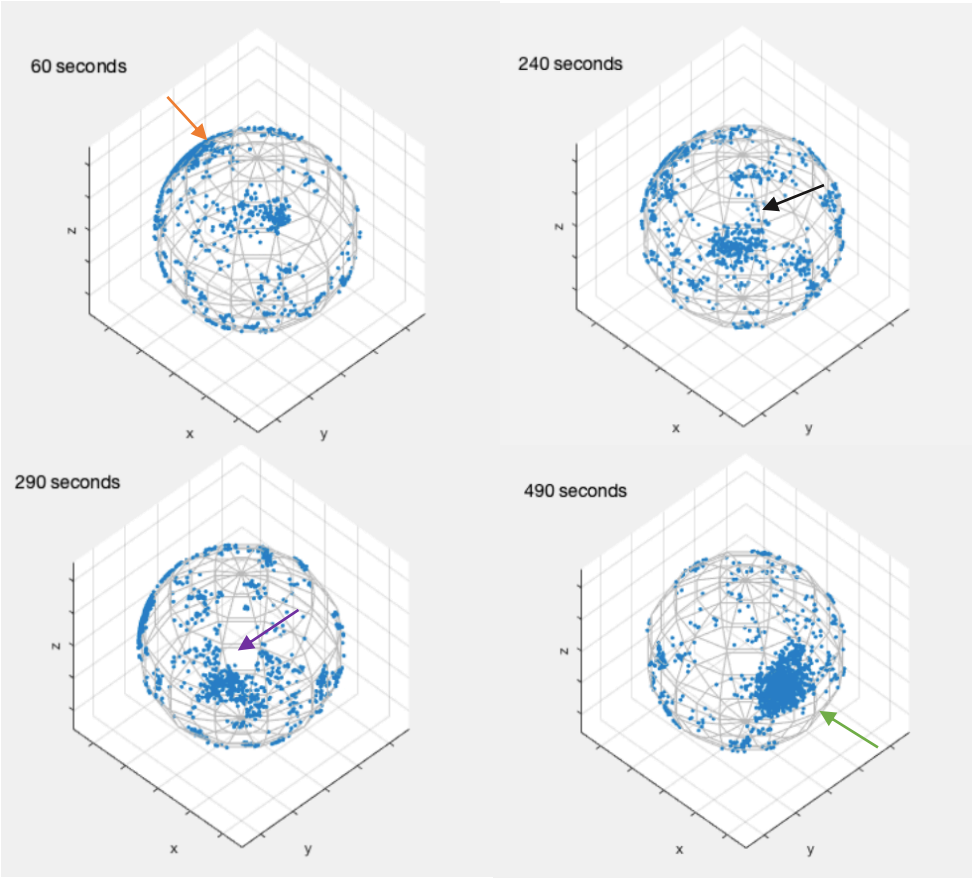

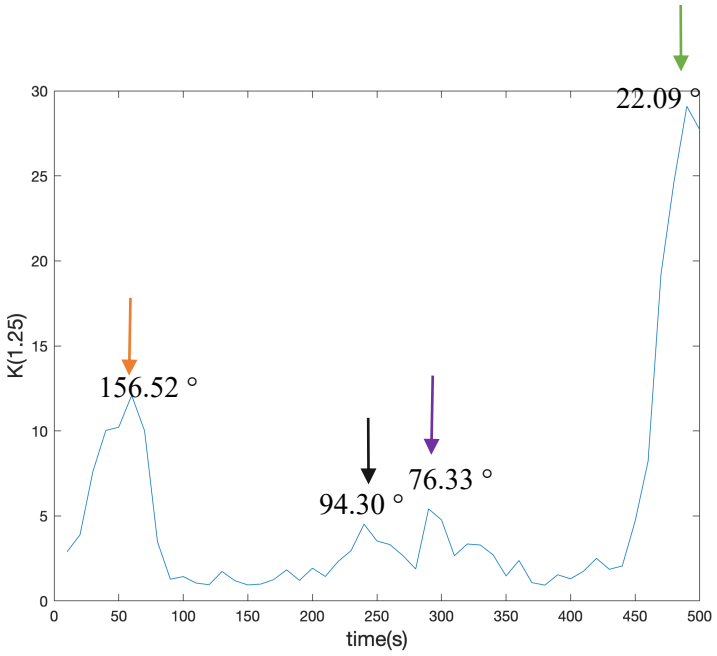
22.09 °
156.52 °
94.30 °
76.33 °
K(1.25)
time(s)
0
5
10
15
20
25
30
0
50
100
150
200
250
300
350
400
450
500

(B)

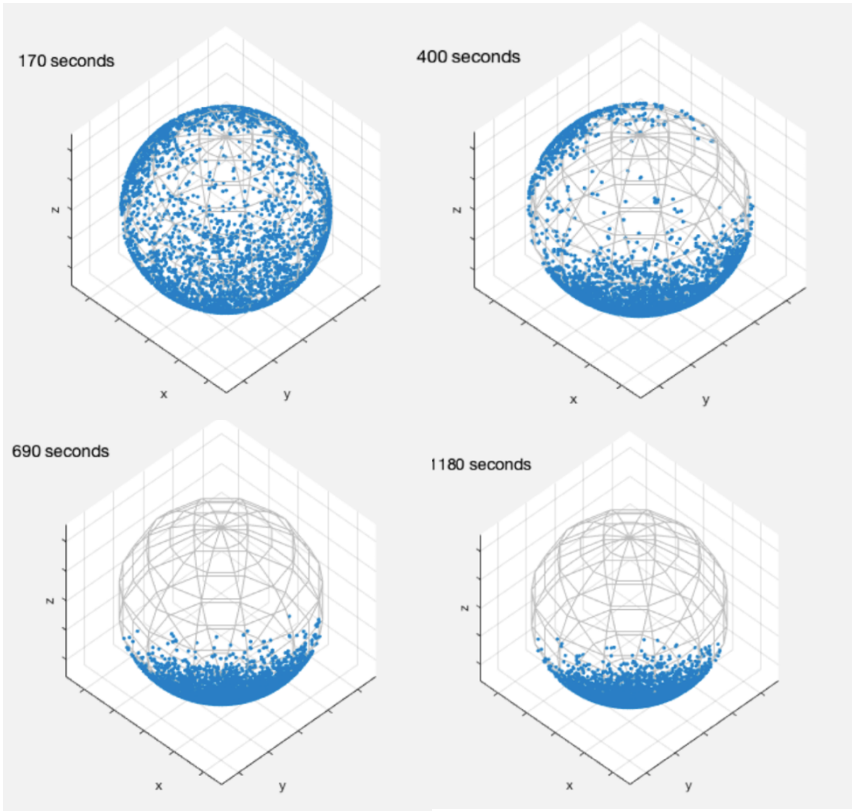
170 seconds
400 seconds
690 seconds
1180 seconds
z
x
y

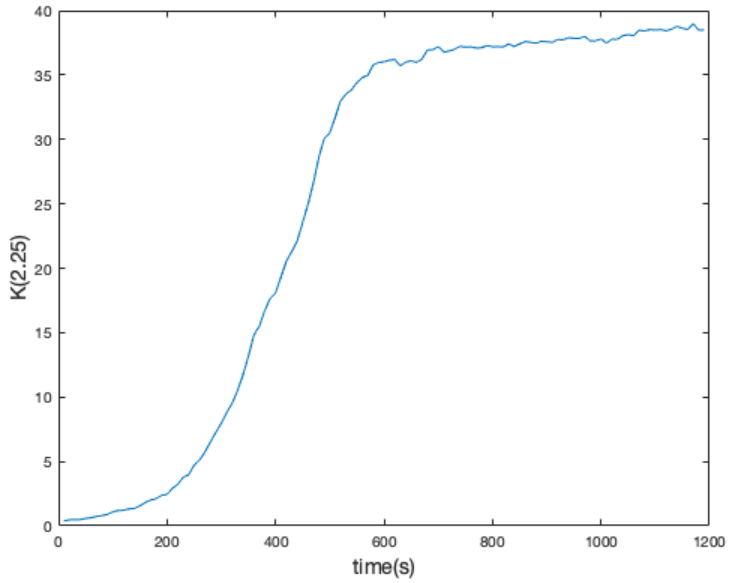

Figure 4. Screenshots of polarity sites in mobile and static models at different time points. Arrows indicate the formation of major polarity sites. The degree of polarity at each time point was quantified by *K(d)*. (A) The mobile model under a 4:6 FarGEFGa gradient. In the graph of *K(1.25) v.s.* time, the polarity angles were calculated for each instant polarity site. (B) The static model taken from Ramirez[28].

The average polarity angles for mobile models under the 1:9 gradient was 38 °. The wandering time was compared between simulated cells in mobile models under the 1:9 gradient with small polarity angles (≤ 38 °) and large angles (> 38 °) (Fig. 5). The average wandering time of the cells with small polarity angles was 148.94 seconds, while that of the cells with large polarity angles was 260.36 seconds. Also, the overall average wandering time of simulated cells in mobile models with polarity angles less than 45 ° was 181.25 s either under a 4:6 or 1:9 gradient. Therefore, in order to polarize to the appropriate direction, it was likely that a mature polarity site should form within 3-4 minutes. Too much wandering time would result in inaccurate polarity establishment.

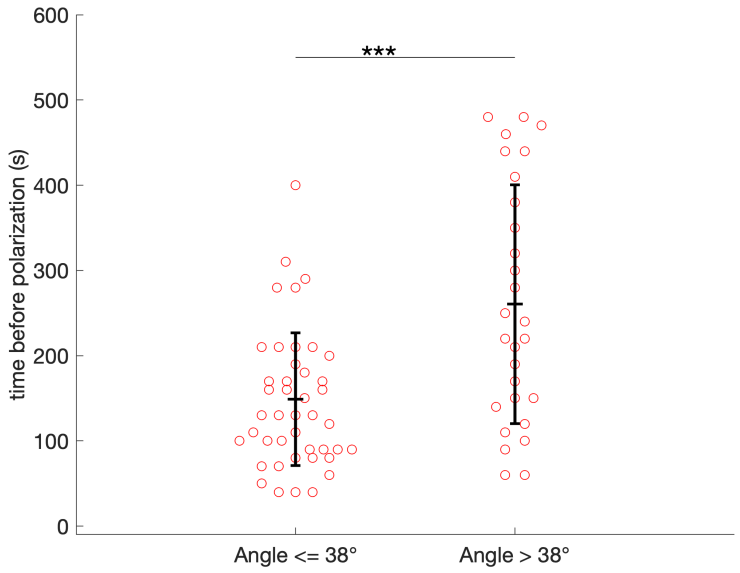

Figure 5. The wandering time before mature polarization. All data were from mobile models under a 1:9 FarGEFGa gradient. The total number of realizations was 75, among which 47 had angles lower than 38 degrees and 28 had angles higher than 38 degrees. KS test, ***: $p < 0.001$.

DISCUSSION

Although wandering, mobile polarization was observed in studies on yeast polarity and mating, it has been difficult to determine how these properties help the cell establish a single polarity site aligned with a shallow, noisy pheromone gradient[20,21,22,23]. In particular, pheromone molecules bound to the receptors only have a difference of 0.5% in the concentration from the cell front and back[14,15]. Our study indicated that wandering polarity sites might help yeast cells interpret the pheromone gradient.

The mobile models had wandering polarization, while the static did not (Fig .4). The mobility of the polarity sites resulted from cytosolic Cdc42 activation, though the detailed mechanism was not clear. A potential explanation is that cytosolic Cdc42 molecules were more dynamic than membrane Cdc42 molecules. Cytosolic Cdc42 had a higher diffusion rate than membrane Cdc42. Once a membrane Cdc42 was deactivated, it diffused so slowly that was activated again by

surrounding GEF molecules. Thereby, the polarity site had the most activated Cdc42 from the start would recruit more and more Cdc42 from other smaller sites via positive feedback until the small sites ran out of Cdc42. Figure 4B was a case in point where the largest site dominated from the beginning till mature polarization, while other small sites disappeared eventually. In contrast to the slowly moving membrane Cdc42, cytosolic Cdc42 could diffuse fast from one end of the cell to another. When we allowed the highly dynamic cytosolic Cdc42 to be activated onto the membrane, the polarity sites could efficiently take Cdc42 directly from the cytosol. Hence, more sites could form simultaneously and compete with each other. It reduced the chance of the formation of an imperishable dominant polarity site, so the initial polarity sites usually could not remain dominant till the end. When exposed to a shallow gradient, mobile models had much smaller polarity angles than the static model (Fig. 3, Column 3&4), which proved that the mobile models responded better to the gradient. Thus, wandering polarization could help yeast cells develop strong polarity sites correctly oriented towards the pheromone gradient.

Additionally, we analyzed the wandering time of mobile models before mature polarization. Here, the mature polarization was defined as the formation of a polarity site whose $K(d) \geq 20$. The mature polarity sites with small polarity angles had wandering time around 2-3 min, and the patches with large polarity angles had significantly longer wandering time over 4 min (Fig. 5). Experiments have shown that during mating, yeast cells are fully polarized around 10 minutes[19], and the first polarity site appeared within 4 minutes of the yeast cell's birth[22]. Thus, our results were on the right scale. Therefore, we concluded that a yeast cell should resolve wandering polarity sites within 3-4 minutes to polarize toward the extracellular pheromone gradient.

With a uniform FarGEFGa gradient, the simulated cells still polarized but in a random direction. It corresponded to the fact that yeast cells could polarize without external spatial cues[11]. It also resonated with studies which proved that positive feedback alone was sufficient to account for the spontaneous establishment of a single site of cell polarity[9,27]. Besides, computational models also confirmed that the positive feedback involving BemGEF were sufficient for yeast cell to polarize in a random direction[18,28].

The characterization of the polarity sites had a few limitations. The establishment of a FarGEFGa gradient was not exactly precise. We fit X coordinates of the molecules in a probability function (See *Models & Methods, Gradient establishment*), but the Y and Z coordinates were generated randomly on the cell membrane. It might result in locally over-concentrated molecules and thus reduce the accuracy of the gradient. However, though not highly precise, this way of gradient establishment efficiently generated three distinct levels of gradients - uniform, shallow (4:6), and sharp (1:9).

CONCLUSION

With particle-based computational modeling, the present study proved that the dynamic, mobile polarity sites could help yeast cells decode the extracellular pheromone gradient against molecular noise. Additionally, we found that the yeast cells that polarized more accurately to the pheromone direction also polarized faster. This study not only illuminated how yeast cells decoded pheromone gradients against molecular noise but also cast light on how eukaryotic cells exposed to molecular noise could polarize appropriately. To confirm our conclusions, future study will be conducted on the characterization of polarity sites on more complicated yeast models under a pheromone-bound GPCR gradient encompassing GPCRs and G proteins as part of the signaling network.

MODELS AND METHODS:

Parameters in particle-based simulations

The static polarity model except the gradient sensing part were taken from Goryachev and Polkhiko[20]. In the static models, all of the parameters except for the number of molecules were taken from Pablo[18]. In the mobile model, the parameters of activation of cytosolic Cdc42 (λ_8 and λ_{10}) were taken from Ramirez[28]. We assume that Cdc24 and Bem1 function as essentially a single unit as done by previous studies[29,18]. The yeast cell was assumed to be a sphere. Table 1 & 2 show parameters used for the D parti3cle-based simulations. Instead of establishing an extracellular pheromone gradient, our simplified model constructed a gradient of membrane FarGEFGa. The model consisted of two pathways that activated cytosolic or membrane Cdc42

(Fig. 1). One pathway involved Bem1-Cdc24 complex, while the other involved Far1-Cdc24 complex. We tested yeast polarity activity respectively under a uniform, shallow, or strong FarGEFGa gradient. Simulation code was developed and run in MATLAB R2018b. Simulations were performed both on desktops and on the University of North Carolina KillDevil computing cluster.

Description	Parameter	Value
$BemGEF_c \rightarrow BemGEF_m$	k_{1a}	5 s^{-1}
$BemGEF_m \rightarrow BemGEF_c$	k_{1b}	10 s^{-1}
$Cdc42D_m + BemGEF_m \rightarrow Cdc42T$	λ_{2a}	4.5 s^{-1}
$Cdc42D_m + FarGEFGa \rightarrow Cdc42T$		
$Cdc42T \rightarrow Cdc42D_m$	k_{2b}	3 s^{-1}
$BemGEF_m + Cdc42T \rightarrow BemGEF42$	λ_{4a}	1.62975×10^{-3} s^{-1}
$BemGEF42 \rightarrow BemGEF_m + Cdc42T$	k_{4b}	20 s^{-1}
$Cdc42D_c \rightarrow Cdc42D_m$	k_{5a}	0.4 s^{-1}
$Cdc42D_m \rightarrow Cdc42D_c$	k_{5b}	0.65 s^{-1}
$BemGEF_c + Cdc42T \rightarrow BemGEF42$	λ_7	1436.7 s^{-1}
$Cdc42D_c + BemGEF42 \rightarrow Cdc42T$	λ_8	2873.39 s^{-1}
$Cdc42D_c + FarGEFGa \rightarrow Cdc42T$	λ_{10}	1000 s^{-1}
Diffusion coefficient in cytoplasm	D_c	15 μm^2 s^{-1}
Diffusion coefficient on membrane	D_m	0.01 μm^2 s^{-1}
Yeast cell diameter	d_{cell}	4.5135 μm
Molecular interaction radii	ρ	0.05 μm
Total Cdc42		5000 particles
Total BemGEF		500 particles
Total FarGEFGa		100 particles
Time step	Δt	0.1 ms
Total time of polarization simulations	T	500 s

Table 1. Parameters used to perform particle-based simulations for mobile models. *c*: cytosol. *m*: membrane.

Description	Parameter	Value
$BemGEF_c \rightarrow BemGEF_m$	k_{1a}'	10 s^{-1}
$BemGEF_m \rightarrow BemGEF_c$	k_{1b}	10 s^{-1}
$Cdc42D_m + BemGEF_m \rightarrow Cdc42T$	λ_{2a}'	5.3 s^{-1}
$Cdc42D_m + FarGEFGa \rightarrow Cdc42T$		
$Cdc42T \rightarrow Cdc42D_m$	k_{2b}'	0.32 s^{-1}
$BemGEF_m + Cdc42T \rightarrow BemGEF42$	λ_{4a}'	8250 s^{-1}
$BemGEF42 \rightarrow BemGEF_m + Cdc42T$	k_{4b}'	10 s^{-1}
$Cdc42D_c \rightarrow Cdc42D_m$	k_{5a}'	36 s^{-1}
$Cdc42D_m \rightarrow Cdc42D_c$	k_{5b}	0.65 s^{-1}
$BemGEF_c + Cdc42T \rightarrow BemGEF42$	λ_7'	256 s^{-1}
$Cdc42D_m + BemGEF42 \rightarrow Cdc42T$	λ_3	15.7 s^{-1}
Diffusion coefficient in cytoplasm	D_c	15 μm^2 s^{-1}
Diffusion coefficient on membrane	D_m'	0.0025 μm^2 s^{-1}
Yeast cell diameter	d_{cell}'	5 μm
Molecular interaction radii	ρ	0.05 μm
Total Cdc42		5000 particles
Total BemGEF		500 particles
Total FarGEFGa		100 particles
Time step	Δt	0.1 ms
Total time of polarization simulations	T	500 s

Table 2. Parameters used to perform particle-based simulations for static models. *c*: cytosol. *m*: membrane.

Gradient establishment

Gradients of either FarGEFGa or pheromone-bound GPCR were established by a way of probability filtering. The gradient direction was set to be the positive direction of *X* axis in the simulated cell. We defined a maximum probability ($Prob_{max}$) and a minimum probability ($Prob_{min}$) of FarGEFGa in the cell along the *X* axis. The linear relationship of the probability of existence of a FarGEFGa molecule and its *X* coordinate was established as in Fig. 6. First, the

coordinates of a membrane FarGEFGa molecule was generated. Then, a random number was generated as the given probability of the molecule. If the given probability was smaller than the probability calculated from the *X* coordinate of this molecule, the coordinates of the molecule were saved; otherwise, this molecule was discarded. This process was repeated until the total number of the molecules reached a number that we wanted.

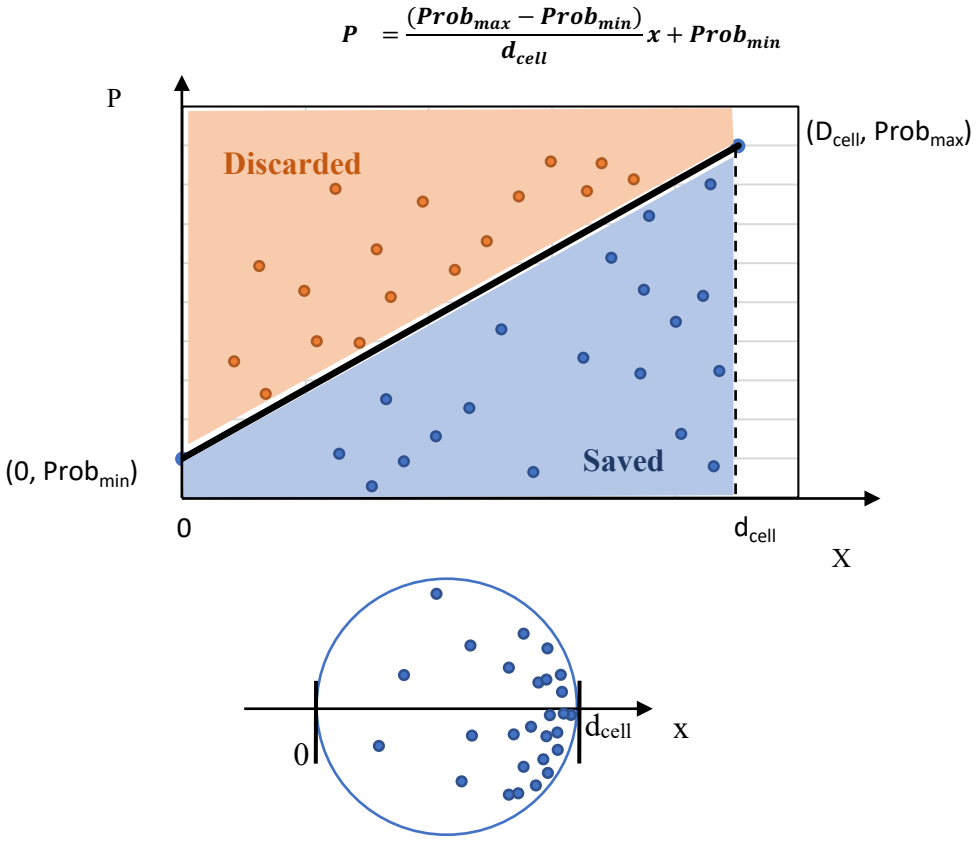

Figure 6. Generation of a FarGEFGa gradient. The linear relationship of the probability of a FarGEFGa molecule and its *X* coordinate was: $P = \left(\frac{Prob_{max} - Prob_{min}}{D_{cell}}\right) x + Prob_{min}$. d_{cell}: diameter of the simulated cell.

Determination of mature polarity

We distinguished between polarized realizations and incompletely polarized realizations with the Ripley's K function with the assumption of complete spatial randomness (CSR) (Eq. 1):

$$K(d) = A\sum_{i=1}^{n}\sum_{j=1,i\neq j}^{n}\frac{I_{t(i,j)}}{n(n-1)} - 2\pi R^2\left[1-\cos\left(\frac{d}{R}\right)\right] \quad \text{(Eq.1)}$$

$$A = 4\pi R^2$$

$$I_{t(i,j)} = \begin{cases} 1 & if\ t(i,j) \leq d \\ 0 & if\ t(i,j) > d \end{cases}$$

where $I_{t(i,j)}$the indicator function. *t(i,j)* is the great-circle distance between the i^{th} and j^{th} points in a data set of *n* points; *d* is the search distance; *A* is the surface area of the sphere containing all points. *R* is the radius of the whole sphere.

K(d) is proportional to the number density in a confined region. In our study, the function was used to determine whether the activated Cdc42 were concentrated at a certain part of the cell. After visual inspection, we defined mature polarization as $K(d) \geq 20$ ($d = 1.25$ for mobile models and 2.25 for static models). We analyzed the polarity angles and wandering time of the first mature polarity site whose *K(d)* reached 20 (Fig. 3, Fig. 5).

Characterization of polarity sites

The angle between the polarization direction and the gradient direction was measured (Fig. 3). When the *K(d)* reached 20 which indicated mature polarization, the average coordinates of activated Cdc42 molecules were calculated. Accordingly, a vector was created between the average coordinates and the center of the cell. Finally, the angle (θ) was calculated between this vector and the gradient vector which was the positive direction of *X* axis.

Statistical analysis

About one-third of the realizations did not polarize in both models. Therefore, to perform reliable statistical analysis, we ran 90 simulations to ensure the number of polarized simulations reached over 50 for each gradient set. The two-sample Kolmogorov–Smirnov (KS) tests were performed in MATLAB via "*kstest2*" function (Fig. 3 & 5). *p*-Values over 0.05 were reported as "n.s. (not significant)"; *p*-values from 0.01 to 0.05 (including 0.01 and 0.05) were reported as

"*(significant)"; *p*-values under 0.001 to 0.01 (including 0.001) were reported as "**(very significant)"; and *p*-values under 0.001 were reported as "***(highly significant)".

ABBREVIATIONS

Bem1	bud emergence 1
Cdc	cell division control
Far1	factor arrest 1
GEF	guanine nucleotide exchange factor
GPCR	G-protein coupled receptor
Ste	sterile
FarGEFGa	Far1-Cdc24 associated with G$\beta\gamma$
BemGEF	Bem-Cdc24 complex
Cdc42T	activated Cdc42, or Cdc42 associated with GTP
Cdc42D	inactivated Cdc42, or Cdc42 associated with GDP

REFERENCES

[1] Arimura, N., & Kaibuchi, K. Neuronal polarity: from extracellular signals to intracellular mechanisms. *Nat Rev* Neurosci **8**, 194–205 (2007).

[2] Matter, K., & Mellman, I. Mechamisms of cell polarity: sorting and transport in epithelial cells. *Current Opinion in Cell Biology*, **6**(4), 545–554 (1994).

[3] Gray, R.S., Roszko, Isabelle., & Solnica-Krezel, L., Planar Cell Polarity: Coordinating Morphogenetic Cell Behaviors with Embryonic Polarity, *Developmental Cell*, **21**(1), 120-133 (2011).

[4] Bourne, H., & Weiner, O. Cell polarity: A chemical compass. *Nature* **419**, 21 (2002).

[5] Weiner, O. D. Regulation of cell polarity during eukaryotic chemotaxis: the chemotactic compass. *Current Opinion in Cell Biology* **14**(2), 196-202 (2002).

[6] Surve, C.R., To, J.Y., Malik, S., Kim, M., & Smrcka, A. V. Dynamic regulation of neutrophil polarity and migration by the heterotrimeric G protein subunits Gαi-GTP and Gβγ. *Science Signaling.* **9** (416), ra22 (2016).

[7] Alvaro, C.G., & Thorner, J. Heterotrimeric G Protein-coupled Receptor Signaling in Yeast Mating Pheromone Response. *J. Biol. Chem*. **291**, 7788 (2016).
[8] Jin, T. GPCR-controlled chemotaxis in Dictyostelium discoideum. *Wiley Interdisciplinary Reviews: Systems Biology and Medicine*, **3**(6), 717–727 (2011).
[9] Altschuler, S., Angenent, S., Wang, Y. et al. On the spontaneous emergence of cell polarity. *Nature* **454**, 886–889 (2008).
[10] Duina, A.A., Miller, M.E., & Keeney, J.B. Budding yeast for budding geneticists: a primer on the Saccharomyces cerevisiae model system. *Genetics*, **197**(1), 33–48 (2014).
[11] Slaughter, B.D., Smith, S.E., Li, R. Symmetry breaking in the life cycle of the budding yeast. Cold Spring Harbor perspectives in biology, **1**(3), a003384 (2009).
[12] McCaffrey, L.M., & Macara, I.G. Widely conserved signaling pathways in the establishment of cell polarity. Cold Spring Harbor perspectives in biology, **1**(2), a001370 (2009).
[13] Chou, C.S., Bardwell, L., Nie, Q., Yi, T.M. Noise filtering tradeoffs in spatial gradient sensing and cell polarization response. *BMC systems biology*, **5**, 196 (2011).
[14] Hegemann, B., Unger, M., Lee, S.S. et al. A Cellular System for Spatial Signal Decoding in Chemical Gradients, *Developmental Cell*, **35**(4), 458-470 (2015).
[15] Arkowitz, R. Chemical Gradients and Chemotropism in Yeast. *Cold Spring Harbor Perspectives in Biology*. **1**(2), a001958 (2009).
[16] Segall, J. E. Polarization of yeast cells in spatial gradients of alpha mating factor. *Proc Natl Acad Sci,* **90**(18), 8332–8336 (1993).
[17] Lakhani V, Elston T.C. Testing the limits of gradient sensing. *PLOS Comput Biol* **13**(2): e1005386(2017).
[18] Pablo, M., Ramirez, S. A., Elston, T. C. Particle-based simulations of polarity establishment reveal stochastic promotion of Turing pattern formation. *PLoS Comput Biol* **14**(3): e1006016 (2018).
[19] Richman, T. J., Sawyer, M. M., & Johnson, D. I. Saccharomyces cerevisiae Cdc42p localizes to cellular membranes and clusters at sites of polarized growth. *Eukaryotic cell*, **1**(3), 458–468 (2002).
[20] Goryachev, A.B., Pokhilko, A.V. Dynamics of Cdc42 network embodies a Turing-type mechanism of yeast cell polarity. *FEBS Lett*. **582**,1437–43 (2008).

[21] Otsuji, M., Ishihara, S., Co, C., Kaibuchi, K., Mochizuki, A., Kuroda, S. A mass conserved reaction-diffusion system captures properties of cell polarity. *PLoS Comput Biol.* **3**(6), e108 (2007).

[22] Howell, A., Jin, M., Wu. C., Zyla, T.R., Elston, T.C., Lew, D. J. Negative Feedback Enhances Robustness in the Yeast Polarity Establishment Circuit, *Cell*, **149**(2), 322-333 (2012).

[23] Wu, C. F., Chiou, J. G., Minakova, M., Woods, B., Tsygankov, D., Zyla, T. R., Savage, N. S., Elston, T. C., & Lew, D. J. Role of competition between polarity sites in establishing a unique front. *eLife*, **4**, e11611 (2015).

[24] Robeson, S.M., Li, A., Huang. C. Point-pattern analysis on the sphere, *Spatial Statistics*,**10**, 76-86 (2014).

[25] Wehrens M., Wolde P.R., Mugler A. Positive feedback can lead to dynamic nanometer-scale clustering on cell membranes. *J Chem Phys*. **141**(20):205102 (2014).

[26] Owen, D. M., Rentero, C., Rossy, J., Magenau, A., Williamson, D., Rodriguez, M, et al. PALM imaging and clus- ter analysis of protein heterogeneity at the cell surface. *J Biophotonics*. **3**(7):446–54 (2010).

[27] Witte, K., Strickland, D., & Glotzer, M. Cell cycle entry triggers a switch between two modes of Cdc42 activation during yeast polarization. *eLife*, **6**, e26722 (2017).

[28] Ramirez, S. & Elston, T.C. Unpublished work.

[29] Woods, B., Lai, H., Wu, C.F., Zyla, T.R., Savage, N.S., & Lew, D.J. Parallel actin-independent recycling pathways polarize Cdc42 in budding yeast. *Curr Biol*. **26**(16), 2114–26 (2016).